Role of alkaline metal in the rare-earth triangular antiferromagnet KYbO2

Franziska Grußler, Mamoun Hemmida, Sebastian Bachus, Yurii Skourski, Hans-Albrecht Krug von Nidda, Philipp Gegenwart, Alexander A. Tsirlin

Angaben zur Veröffentlichung / Publication details:

Grußler, Franziska, Mamoun Hemmida, Sebastian Bachus, Yurii Skourski, Hans-Albrecht Krug von Nidda, Philipp Gegenwart, and Alexander A. Tsirlin. 2023. "Role of alkaline metal in the rare-earth triangular antiferromagnet KYbO2." *Physical Review B* 107 (22): 224416. https://doi.org/10.1103/physrevb.107.224416.

Editors' Suggestion

Role of alkaline metal in the rare-earth triangular antiferromagnet $KYbO_2$

Franziska Grußler,[1,*] Mamoun Hemmida,[2] Sebastian Bachus,[1] Yurii Skourski,[3] Hans-Albrecht Krug von Nidda,[2] Philipp Gegenwart,[1] and Alexander A. Tsirlin[1,4,†]

[1]*Experimental Physics VI, Center for Electronic Correlations and Magnetism, University of Augsburg, 86135 Augsburg, Germany*
[2]*Experimental Physics V, Center for Electronic Correlations and Magnetism, University of Augsburg, 86135 Augsburg, Germany*
[3]*High Magnetic Field Laboratory (HLD-EMFL, Helmholtz-Zentrum Dresden-Rossendorf, 01328 Dresden, Germany*
[4]*Felix Bloch Institute for Solid-State Physics, Leipzig University, 04103 Leipzig, Germany*

(Received 23 March 2023; revised 12 May 2023; accepted 17 May 2023; published 15 June 2023)

We report crystal structure and magnetic behavior of the triangular antiferromagnet $KYbO_2$, the A-site substituted version of the quantum spin liquid candidate $NaYbO_2$. The replacement of Na by K introduces an anisotropic tensile strain with 1.6% in-plane and 12.1% out-of-plane lattice expansion. Compared to $NaYbO_2$, both Curie-Weiss temperature and saturation field are reduced by about 20% as the result of the increased Yb-O-Yb angles, whereas the g tensor of Yb^{3+} becomes isotropic with $g = 3.08(3)$. Field-dependent magnetization shows the plateau at $\frac{1}{2}$ of the saturated value and suggests the formation of the up-up-up-down field-induced order in $KYbO_2$ in contrast to the more common $\frac{1}{3}$ plateau with the up-up-down order that has been reported in the isostructural Yb^{3+} selenides.

DOI: 10.1103/PhysRevB.107.224416

I. INTRODUCTION

Since Anderson proposed the formation of a quantum spin liquid (QSL) in triangular antiferromagnets [1], the scientific community struggled to find a real-life material to investigate this intriguing state of matter. QSL boasts high spin entanglement combined with strong quantum fluctuations and absence of magnetic order down to the lowest temperatures. Furthermore, fractionalized excitations of the QSL may have far-reaching implications for quantum technology [2–4].

In 2015, the research on triangular QSLs was enlivened by the discovery of $YbMgGaO_4$ [5]. The absence of magnetic order down to at least 48 mK [6,7], the $C_v \propto T^{2/3}$ power-law behavior of the specific heat [8,9], and the observation of an excitation continuum in the inelastic neutron scattering spectra [10–12] marked $YbMgGaO_4$ as a promising example of the U(1) QSL. However, effects of structural randomness strongly influence this putative QSL behavior because the disorder in the nonmagnetic Mg/Ga layer creates a random charge environment of the Yb^{3+} ions, thus leading to a distribution of local magnetic moments and exchange interactions [13–15].

Despite these potential complications, $YbMgGaO_4$ sparked the interest in the rare-earth-based triangular antiferromagnets, especially those with Yb^{3+} as the pseudospin-$\frac{1}{2}$ magnetic ion. Triangular antiferromagnets $AYbX_2$ (A = Li, Na, K, Rb, Cs; and X = S, Se, O) have become the focus of research over the past years [16–21], since most of them are believed to be free from any structural disorder. With more and more members of the $AYbX_2$ family being prepared and investigated [18,22–30], one seeks to understand in what manner the single-ion magnetism of Yb^{3+} and the interactions in the triangular Yb^{3+} layers are affected by the surrounding ions. The $YbMgGaO_4$ case has shown that the surrounding nonmagnetic atoms are not simple observers. They can have crucial influence on the low-temperature behavior and formation of a QSL [15].

Here, we address this question by a detailed comparison between $NaYbO_2$, reported previously as the disorder-free QSL candidate [17–19], and isostructural $KYbO_2$ [31] that has not been on the radar of magnetism research. The Li compound with the same stoichiometry is also known, but it features a different crystal structure and, consequently, the three-dimensional diamond spin lattice [32]. In $NaYbO_2$, Yb^{3+} features a Kramers doublet ground state separated from the first excited doublet by $\Delta = 34.8$ meV ≈ 400 K [17,19]. Below 50 K, an effective spin-$\frac{1}{2}$ description holds, albeit with the anisotropic g tensor [18]. Magnetic interactions between the effective spins are on the order of 5 K, yet specific heat and muon spin relaxation measurements confirm the absence of magnetic long-range order and the presence of spin dynamics down to at least 70 mK in zero field [17,19]. Long-range magnetic order is induced in the magnetic fields above 3 T [18,19]. In the following, we track how these features evolve upon replacing sodium in $NaYbO_2$ with potassium, and thus reveal the role of alkaline metals in the $AYbX_2$ family of triangular antiferromagnets.

II. METHODS

Sample preparation. Polycrystalline $KYbO_2$ was synthesized by a solid-state reaction using KO_2 and Yb_2O_3 as starting materials. The reagents were weighed and ground in an agate mortar in an argon-filled glovebox to prevent a

*franziska.grussler@physik.uni-augsburg.dee
†altsirlin@gmail.com

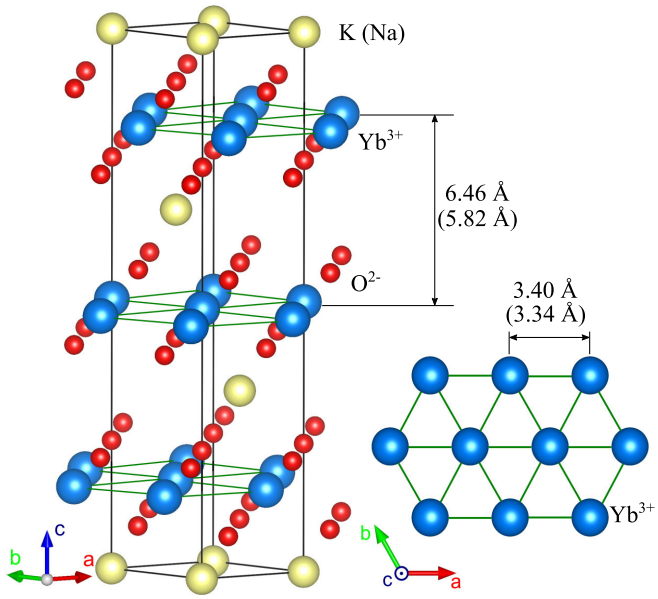

FIG. 1. Schematic crystal structures of $KYbO_2$ and $NaYbO_2$. The values for the inter and intralayer Yb-Yb distances for $KYbO_2$ are determined from the crystal structure refinement at 10 K, see below. The values for $NaYbO_2$ [17] are given in brackets.

reaction of KO_2 with air moisture. An excess of 75% KO_2 was used similar to the approach in Ref. [31]. The powdered reagents were filled into a platinum crucible, placed in a horizontal furnace, heated to 650 °C, held at this temperature for 16 h, and subsequently cooled down to room temperature. The reaction was performed using an argon flow of 20 sccm. The finished product was stored under argon atmosphere since it rapidly decomposes in contact with air moisture. For a direct comparison with $KYbO_2$, the polycrystalline sample of $NaYbO_2$ was prepared similar to the previous study [17].

Crystal structure. Synchrotron x-ray diffraction measurements were performed to determine the crystal structure (Fig. 1). Diffraction data were collected at the MSPD beamline [33] (ALBA, Spain) using the multianalyzer setup and the wavelength of $\lambda = 0.32525$ Å at the constant temperature of 10 K. To reduce preferred-orientation effects, the powder sample was placed into a thin-wall glass capillary and spun during the measurement.

Magnetic characterization. Temperature-dependent magnetic susceptibility was measured using the SQUID magnetometer from Quantum Design (MPMS 3) from 2 to 300 K at 1 T (ZFC) and between 0.4 and 2 K in various magnetic fields between 1 and 5 T utilizing the ^{3}He cooling stage. Field-dependent magnetization measurements up to 7 T were performed at various temperatures between 0.4 K and 1 K using the MPMS with the ^{3}He cooling stage. The Quantum Design PPMS equipped with the vibrating sample magnetometer option provided an extension of the magnetic field up to 14 T at 2 K. The field-dependent magnetization up to 40 T was measured at 0.54 K using a triply compensated extraction magnetometer within a 50 T mid-length-pulse magnet at the High Magnetic Field Laboratory Dresden.

Specific heat measurements. The specific heat of $KYbO_2$ as well as $NaYbO_2$ was measured by thermal relaxation method between 0.5 and 30 K using the PPMS from Quantum Design with the ^{3}He insert at various magnetic fields. Zero-field measurements were extended up to 300 K using the standard ^{4}He setup. In the case of $NaYbO_2$, a dilution refrigerator has been used to extend the temperature range down to 70 mK. The specific heat in fields up to 8 T has been determined by a thermal relaxation method. Further details can be found in Ref. [17], where selected low-field data ($B \leqslant 1.25$ T) for $NaYbO_2$ have already been reported.

ESR measurements. The electron spin resonance (ESR) measurements were performed in a continuous wave spectrometer (Bruker ELEXSYS E500) at X-band frequency ($\nu \approx 9.35$ GHz) in the temperature region $4 \leqslant T \leqslant 300$ K using a continuous He gas-flow cryostat (Oxford Instruments). ESR detects the power P absorbed by the sample from the transverse magnetic microwave field as a function of the static magnetic field H. The signal results from magnetic dipole transitions between the Zeeman levels of the electron spins. The signal-to-noise ratio of the spectra is improved by recording the derivative dP/dH using a lock-in technique with field modulation. The measurement was done on a polycrystalline sample fixed in a quartz tube with paraffin.

III. RESULTS

A. Crystal structure

Our synchrotron XRD data confirm the $R\bar{3}m$ space group and the high crystallinity of $KYbO_2$. Two minor impurity phases also found in the sample, Yb_2O_3 and $KOH \cdot H_2O$ [Fig. 2(a) and 2(c)], are decomposition products, as the capillary was shortly exposed to air upon the insertion into the cryostat. Crystal structure refinement reveals low atomic displacement parameters (ADPs), most notably, the low ADP of Yb, in contrast to $YbMgGaO_4$ where Yb ADP remains sizable, about 0.01 Å^2 at 100 K [5], and signals local displacements caused by the random distribution of Mg^{2+} and Ga^{3+} in the structure. On the other hand, the $KYbO_2$ structure should be fully ordered, similar to $NaYbO_2$.

In Tables I and II, we compare the structural parameters of $NaYbO_2$ and $KYbO_2$. The replacement of Na by K leads to a highly anisotropic lattice expansion with the 1.6% increase in a and 12.1% increase in c. This anisotropy can be traced back to the rigid nature of the [YbO_2] layers that undergo only a weak expansion demonstrated by the 0.8% increase in the Yb-O distances. This expansion is insufficient to account for the 1.6% increase in the Yb-Yb distances, so the Yb-O-Yb angles increase too. They, in turn, affect the local environment of Yb^{3+}, because the Yb-O-Yb and O-Yb-O angles are equal by symmetry.

Overall, we find that negative pressure introduced by the K substitution causes both expansion (increase in the Yb-O distances) and flattening (increase in the Yb-O-Yb angles) of the triangular [YbO_2] layers. In contrast, hydrostatic pressure effect reported for $YbMgGaO_4$ [34] leads to a uniform compression wherein the Yb-O distances shrink while the Yb-O-Yb angles remain almost constant. The tensile strain introduced by the chemical substitution is thus highly anisotropic.

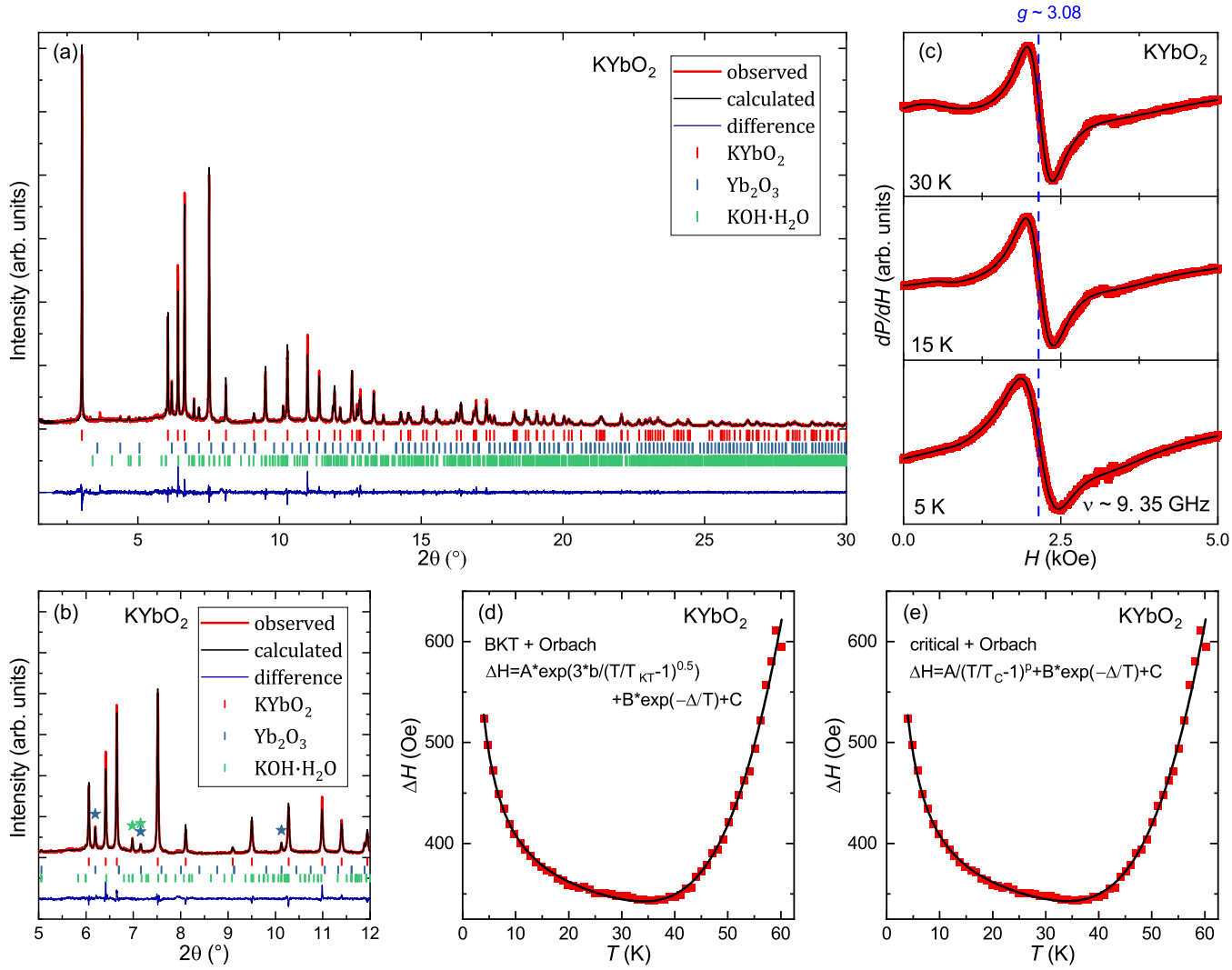

FIG. 2. (a) Structure refinement using the synchrotron diffraction pattern at 10 K. (b) Zoom in to the angular range between 5 and 12° where the reflections from the impurity phases are marked with stars. (c) ESR spectra of $KYbO_2$ taken at the X-band frequency for selected temperatures. The solid line indicates the fit with the field derivative of a symmetric Lorentz line. (d), (e) Fits of the ESR linewidth with an Orbach process at high temperatures and two possible models at low temperatures (see text for details).

B. *g* values

Local magnetism of the Yb^{3+} ions is revealed by the ESR measurements. After subtracting the cavity background, the Yb-ESR lines are well described by the field derivative of a single Lorentzian [see Fig. 2(b)]. Distortions between 2.8 and 3.5 kOe are due to the fact that the background could not be perfectly subtracted, because of slightly different quality factor with and without the sample. The broad shoulder at low fields was taken into account by a second Lorentzian derivative, but it is ascribed to the impurity phase. On increasing temperature, the ESR signal becomes very broad due to an Orbach process that includes population of excited crystal-electric-field (CEF) levels of Yb^{3+} [35].

TABLE I. Comparison of $NaYbO_2$ and $KYbO_2$. The lattice parameters, Yb-O and (Na/K)-Yb distances are given in Å, while the bridging angles Yb-O-Yb are expressed in degrees. The powder-averaged g value is determined from ESR. The van Vleck contribution to the susceptibility, χ_{vv}, is determined from the linear part of the high-field magnetization and given in units of emu/mol. The characteristic temperature θ (in K) is obtained from the Curie-Weiss fits after subtracting χ_{vv}. The values for $NaYbO_2$ are taken from Ref. [17] and from Ref. [18] (g_{ESR}).

	a	c	Yb-O dist.	∠Yb-O-Yb	(Na/K)-Yb dist.	g_{ESR}	χ_{vv}	θ
$NaYbO_2$	3.34481(4)	16.4585(2)	2.25537(3)	95.723(1)°	3.35466(3)	2.86(7)	0.00564(6)	−6.4(3) K
$KYbO_2$	3.39731(4)	18.453(3)	2.27232(3)	96.756(1)°	3.64786(5)	3.08(3)	0.00399(1)	−5.4(2) K

TABLE II. Atomic positions and atomic displacement parameters U_{iso} determined from the structure refinement against the 10 K synchrotron data. The results for $NaYbO_2$ are from Ref. [17].

atoms	x/a	y/b	z/c	U_{iso}(Å^2)
$NaYbO_2$				
O	0	0	0.2375(1)	0.0007(4)
Yb	0	0	0.5	0.00015(3)
Na	0	0	0	0.0032(3)
$KYbO_2$				
O	0	0	0.2288(3)	0.005(1)
Yb	0	0	0.5	0.0015(2)
K	0	0	0	0.0046(5)

Interestingly, only one symmetric ESR line is observed in $KYbO_2$. This stands in contrast to the previous reports on other $AYbX_2$ compounds. The g tensors of both $NaYbS_2$ and $NaYbSe_2$ show a strong easy-plane anisotropy, with $g_\parallel \leqslant 1.0$ and $g_\perp \simeq 3.2$ [18,30,36]. A similar easy-plane anisotropy is observed in $NaYbO_2$ where $g_\parallel = 1.75(3)$ and $g_\perp = 3.28(8)$ were reported on a polycrystalline sample [37]. On the other hand, our data suggest an almost isotropic $g \simeq 3.08(3)$ in $KYbO_2$. This change parallels the structural evolution of the $[YbO_2]$ layers that undergo an anisotropic expansion. Consequently, the composition of the ground-state Kramers doublet of Yb^{3+} should change, and its g values are modified accordingly.

Temperature dependence of the ESR linewidth is shown in Figs. 2(d) and 2(e). The broadening at high temperatures is ascribed to the aforementioned Orbach process, $\Delta H \propto \exp(-\Delta/T)$. The resulting energy gap $\Delta \simeq 350$ K between the ground-state Kramers doublet and first excited CEF level is quite close to that determined for $NaYbO_2$ ($\Delta = 350$ K [35] and $\Delta = 320$ K [37]).

At low temperatures, two possible models are considered. One interpretation relies on the classical critical behavior in the vicinity of a phase transition, $\Delta H \propto (T/T_c - 1)^{-p}$ with the critical temperature T_c [Fig. 2(e)]. The other interpretation [Fig. 2(d)] assumes the proximity to a Berezinskii-Kosterlitz-Thouless (BKT) transition with $\Delta H \propto \exp[3b/((T/T_{KT}) - 1)^{0.5}]$, the Kosterlitz-Thouless (KT) temperature T_{KT}, and $b = \pi/2$ [38]. The BKT interpretation was previously applied to the $ACrO_2$ triangular antiferromagnets (A = H, Li, Na) [39], although later studies challenged this scenario [40]. While there are no direct indications for a significant XY anisotropy

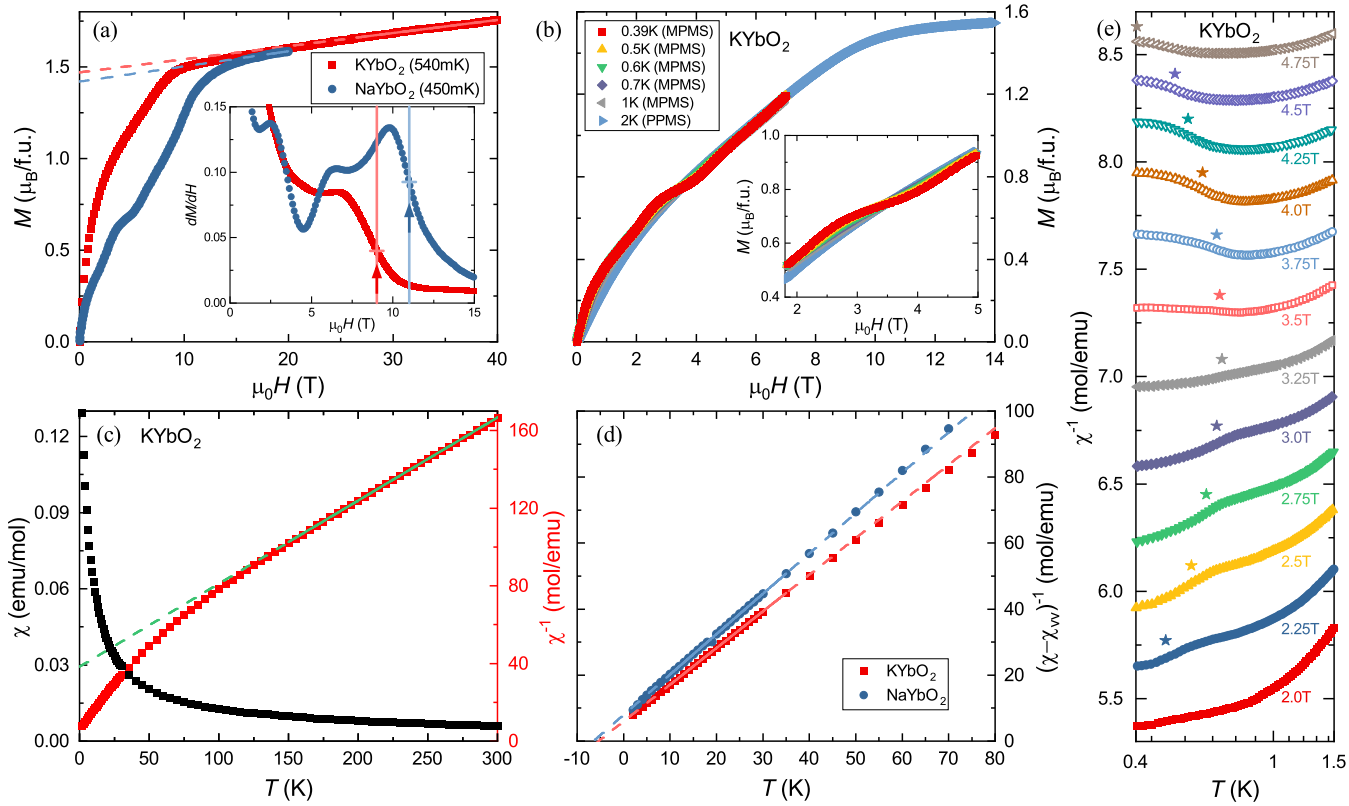

FIG. 3. (a) Magnetization of $KYbO_2$ and $NaYbO_2$ measured at 0.54 K up to 40 T and 0.45 K up to 20 T, respectively. The linear fits are used to determine the Van Vleck contribution. The magnetization data of $NaYbO_2$ was adapted from [17] by scaling the high-field measurement to our ^{3}He MPMS measurements (see Fig. 7). The inset shows the field derivative of the magnetization with the arrows indicating the respective saturation fields. (b) Magnetization of $KYbO_2$ measured with the MPMS and PPMS (blue triangles, 2 K) at various temperatures. At low temperatures, a plateau is clearly observed between 2 and 5 T at about half of the saturation magnetization. (c) Magnetic susceptibility and inverse magnetic susceptibility for $KYbO_2$ measured in the applied field of 1 T. The green line represents the high-temperature Curie-Weiss fit. (d) Low-temperature Curie-Weiss fit for $NaYbO_2$ and $KYbO_2$ after the subtraction of the van Vleck term χ_{vv}. (e) Low-temperature susceptibility of $KYbO_2$ measured at various magnetic fields. The transition temperatures are indicated by stars.

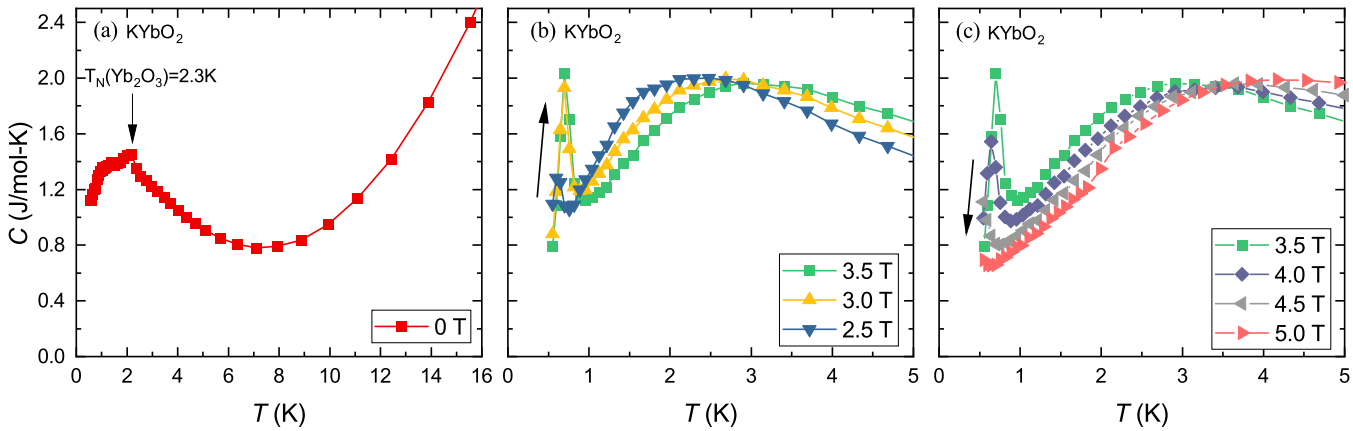

FIG. 4. (a) Specific heat of $KYbO_2$ measured in zero field. The 2.3 K anomaly corresponds to the Yb_2O_3 impurity phase. (b) Magnetic order appears for magnetic fields larger than 2.5 T. The peak becomes more pronounced with increasing the field up to 3.5 T. (c) For fields larger than 3.5 T the peak becomes smaller and shifts to lower temperatures.

in $KYbO_2$, we used both models to demonstrate: (i) equally good fits that make it hard to conclude on the applicability of the BKT scenario from the ESR data alone; (ii) similarity of the critical temperatures, $T_{KT} = 0.14$ K and $T_c = 0.15$ K, extracted from both fits. We also note that the critical exponent $p = 0.77$ is similar to the $T^{-0.75}$ power-law behavior established in sibling compounds [35,36].

C. Thermodynamic properties

Inverse magnetic susceptibility of $KYbO_2$ shows linear behavior at high temperatures and gradually changes slope below 150 K [see Fig. 3(c)]. The Curie-Weiss fit of the linear part returns the Curie-Weiss temperature $\theta = -89.6$ K and the effective moment of $\mu_{\text{eff}} = 4.32\mu_B$, which is similar to the free-electron value of $4.54\mu_B$ for Yb^{3+}.

At low temperatures, the ground-state Kramers doublet of Yb^{3+} is responsible for the pseudospin-$\frac{1}{2}$ behavior, whereas the effect of higher-lying CEF levels is taken into account by the temperature-independent van Vleck term χ_{vv} [15]. We determine its value from field-dependent magnetization that shows the linear increase above the saturation field [Fig. 3(a)]. In $KYbO_2$, the saturation is observed around 9 T, whereas the linear part at high magnetic fields (27 − 40 T) yields $\chi_{vv} = 0.00715\ \mu_B/\text{T} = 0.00399$ emu/mol. The saturation magnetization of 1.47 μ_B/f.u. can be deduced after correcting $M(H)$ for the van Vleck contribution. This value is in a good agreement with the saturation magnetization $M_{\text{sat,ESR}} = gS = 1.54\ \mu_B$/f.u. calculated using the g value from ESR and $S = \frac{1}{2}$.

In order to gauge magnetic interactions between the ground-state Kramers doublets, we subtract χ_{vv} from the experimental susceptibility and find the linear regime in $(\chi - \chi_{vv})^{-1}$ between 10 and 50 K [Fig. 3(d)]. The corresponding effective moment of $2.68\mu_B$ perfectly matches the expected value of $g\sqrt{S(S+1)} = 2.67\ \mu_B$ with $g = 3.08$ and $S = \frac{1}{2}$, while the negative Curie-Weiss temperature of $\theta_{CW} = -5.4$ K indicates antiferromagnetic interactions.

It is instructive to compare $(\chi - \chi_{vv})^{-1}$ between $KYbO_2$ and $NaYbO_2$ [Fig. 3(d)]. The K compound shows a lower slope because of the higher effective moment, which is determined by $g = 3.08$, to be compared with the powder-averaged $g_{av} = 2.86$ in $NaYbO_2$. On the other hand, the absolute value of the Curie-Weiss temperature is reduced upon replacing Na with K. A similar trend can be seen in the saturation field that decreases from 11 T in $NaYbO_2$ [17,37] to about 9 T in $KYbO_2$.

We now turn to the low-temperature behavior and discuss the plateau feature, which is observed in $M(H)$ below 0.7 K. This slightly tilted plateau is clearly seen in the MPMS data measured in static fields below 0.7 K [Fig. 3(b)]. The absence of the plateau in the pulsed-field data [Fig. 3(a)] may be due to the slight sample heating during the pulse. Magnetization plateaus have been observed in many of the $AYbX_2$ compounds when ordered spin states are induced by the applied field. In $AYbSe_2$ (A = Na, K, Rb, Cs), measurements on single crystals showed that the plateau appears for in-plane magnetic fields only and corresponds to $\frac{1}{3}$ of the saturation magnetization [18,28]. Neutron scattering experiments in the applied field confirmed the up-up-down (*uud*) nature of the magnetic order [41,42]. The same *uud* order was observed by neutrons in $NaYbO_2$ [19], although magnetization at the plateau reaches $\frac{1}{2}$ of the saturation value [17] and exceeds expected magnetization of the *uud* state. This discrepancy might be caused by the anisotropic nature of the Yb^{3+} moments. Interestingly, magnetization of $KYbO_2$ at the plateau, about 0.7 μ_B/f.u., also reaches $\frac{1}{2}$ of the saturation value. Given the isotropic nature of the Yb^{3+} moments, this result speaks against the formation of the *uud* phase. An up-up-up-down (*uuud*) field-induced order would be a more likely candidate.

The field-induced magnetic order also manifests itself as a kink in the low-temperature susceptibility shown in Fig. 3(e). For fields below 3.5 T a downward turn in $\chi^{-1}(T)$ is observed, while for fields larger than 3.5 T, inverse susceptibility shows an upward curvature. The transition temperature is determined via the respective maximum or minimum in the first derivative of $\chi^{-1}(T)$ and increases from 0.49 K in an applied field of 2.25 T to 0.71 K at 3.25 T. Above 3.25 T the transition temperature decreases and disappears below the measurement range above 4.75 T.

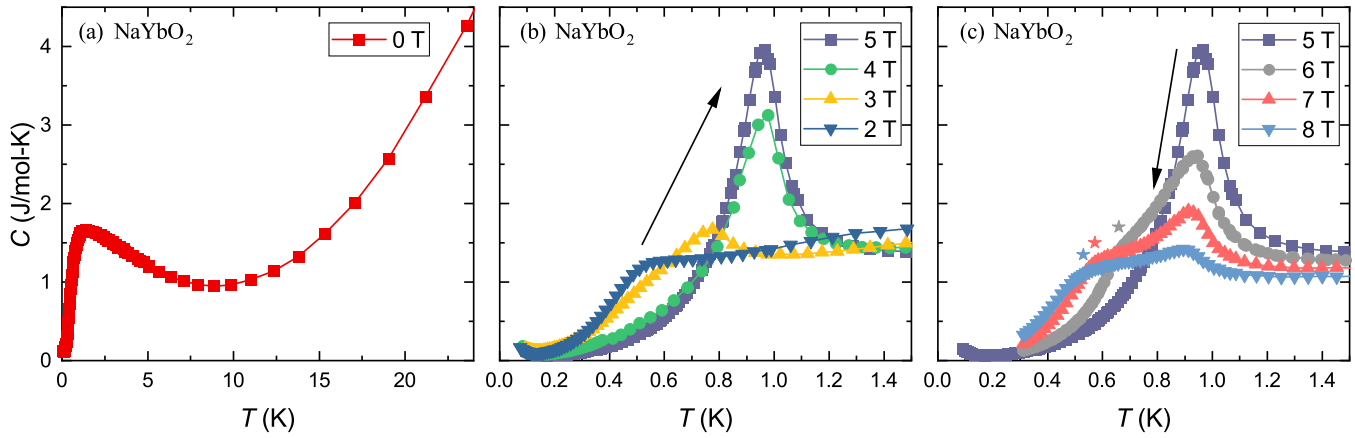

FIG. 5. (a) Measurements of the specific heat of $NaYbO_2$ in zero field. (b) Magnetic order is first observed in a magnetic field of 3 T. The transition is shifted to higher temperatures with increasing magnetic field up to 5 T. (c) Further increasing the magnetic field leads to a decrease in the transition temperature. The stars mark the lower-temperature shoulder that appears above 6 T.

Field-induced magnetic order is further monitored by specific heat measurements performed with the ^{3}He insert down to 0.5 K (see Fig. 4). No magnetic order is observed in zero field, similar to $NaYbO_2$. Specific heat reveals a broad maximum indicative of short-range magnetic order, as well as a small anomaly around 2.3 K due to the magnetic ordering transition in the Yb_2O_3 impurity phase [43].

Magnetic field systematically shifts the specific heat maximum toward higher temperatures, the same can be observed for $NaYbO_2$ (see Fig. 5). Above 2 T, field-induced long-range magnetic order in $KYbO_2$ is revealed by a λ-type anomaly. The ordering peak shifts to higher temperatures on increasing the field up to 3 T, then shifts to lower temperatures on further increasing the field up to 4.5 T. At 5 T, the onset of the ordering peak is still visible but the peak itself lies below our measurement range. A qualitatively similar behavior is observed in $NaYbO_2$ (Fig. 5).

By tracing the λ-type anomaly in different magnetic fields, the start and end of the magnetization plateau [determined from the maxima in the second derivative of $M(H)$], and the kink in the magnetic susceptibility, we construct field-temperature phase diagrams for both $KYbO_2$ and $NaYbO_2$ (Fig. 6). They show that the stability region of the plateau phase in the K compound is merely scaled down with respect to the Na one, in line with the weaker magnetic interactions in the former.

Above 5 T, $NaYbO_2$ displays a clear splitting between the plateau end measured by $M(H)$ and the magnetic ordering transition measured by $C_p(T)$. This splitting indicates that another ordered phase should appear above the plateau region. It may be a noncollinear V-type phase that has been pinpointed in Co-based triangular antiferromagnets [44] and also proposed theoretically [45,46]. The $KYbO_2$ data show no clear signatures of such a phase, although the temperature range of our measurements was probably insufficient for detecting it. Experiments below 0.5 K would be necessary to clarify this point.

IV. DISCUSSION

The A-site chemical substitution in the QSL candidate $NaYbO_2$ has two main implications. First, the g tensor of Yb^{3+} becomes symmetric. Second, magnetic interaction strength decreases. The latter effect can be ascribed to the increased Yb-O-Yb angle. Indeed, with the angle of 96.76° $KYbO_2$ takes an intermediary position between $NaYbO_2$ (95.72°) and $YbMgGaO_4$ (100.36°). The absolute value of the powder-averaged Curie-Weiss temperature θ_{CW} correspondingly decreases from 6.4 K in $NaYbO_2$ [17] to 5.4 K in $KYbO_2$ and 2.3 K in $YbMgGaO_4$ [5]. This reduction further manifests itself in the lower saturation field and in the shrinkage of the plateau region in the phase diagram (Fig. 6).

The effect on the g value is more subtle. It is probably related to the change in the local environment of Yb^{3+} that determines the CEF levels and the composition of the ground-state Kramers doublet. Interestingly, in $KYbO_2$ the trigonal distortion of the YbO_6 octahedra increases, but at the same time the alkaline-metal ions move further away from Yb^{3+}. The A-Yb distance increases from 3.36 Å in $NaYbO_2$ to 3.65 Å in $KYbO_2$. A similar effect was reported in $AgYbO_2$ [35] where the smaller Na^+ is also replaced by the larger ion (Ag^+). However, that sample showed a very broad ESR line with $g = 3.1(5)$, while our $KYbO_2$ sample reveals a more narrow line, which is comparable in width with the line of $NaYbO_2$, yet isotropic with $g = 3.08(3)$.

The isotropic nature of the local moment simplifies interpretation of the data collected on powder samples. Indeed, easy-plane anisotropy of the g tensor for $NaYbO_2$ [$g_\parallel = 1.75(3)$ and $g_\perp = 3.28(8)$] suggests that the magnetization curve of this compound should be a superposition of the signals obtained for different directions of the applied field. This explains the residual curvature observed in $M(H)$ between 11 and 16 T because the $H\|c$ component may have a higher saturation field due to the lower g value. This anisotropy should also affect the magnetization value at the plateau and precludes its unambiguous assignment to the *uud* ($M_{sat}/3$) or *uuud* ($M_{sat}/2$) phases. In the case of $KYbO_2$, we do not observe any significant residual curvature above the saturation field of 9 T, as the g value is isotropic. Then the magnetization of about 0.7 μ_B/f.u. at the plateau serves as the fingerprint of the *uuud* state that distinguishes $KYbO_2$ from the $AYbSe_2$ selenides with the field-induced *uud* order.

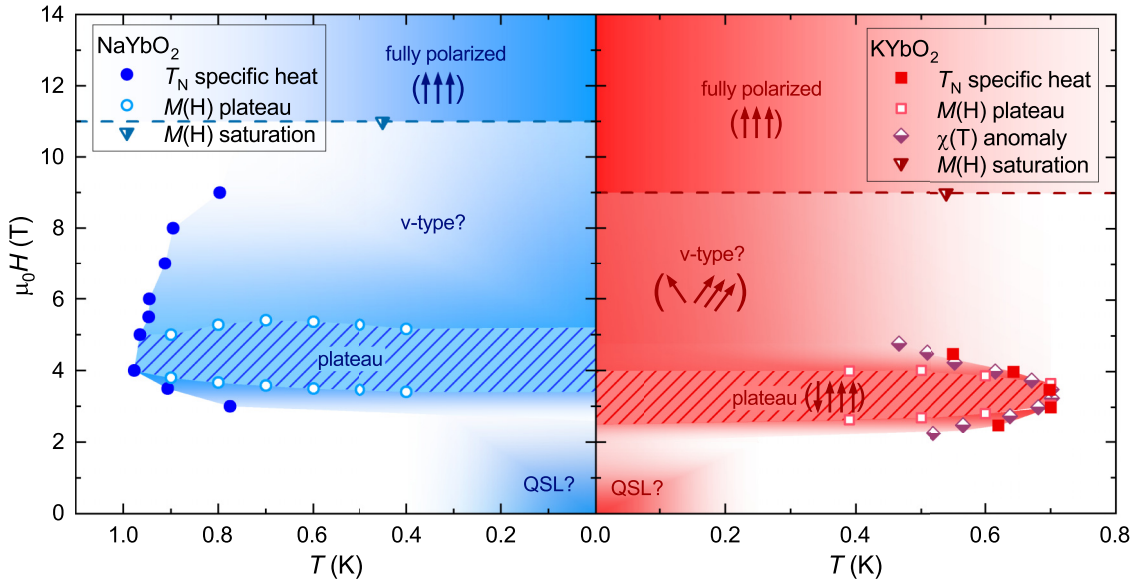

FIG. 6. Comparison of the field-temperature phase diagrams for $NaYbO_2$ (blue, left) and $KYbO_2$ (red, right) derived from the specific heat (filled symbols), field-dependent magnetization (open symbols) measurements, and temperature-dependent magnetic susceptibility (partially filled symbols) measurements.

The *uuud* state is indeed expected [45] in triangular antiferromagnets with $J_2/J_1 > 0.125$, where J_1 and J_2 stand for the nearest-neighbor and next-nearest-neighbor couplings, respectively. A sizable J_2 is thus a precondition for the formation of the field-induced *uuud* state. Recent neutron scattering studies suggested $J_2/J_1 = 0.04 - 0.05$ in the $AYbSe_2$ selenides [41,42]. This interaction regime is consistent with the $\frac{1}{3}$ magnetization plateau and the field-induced *uud* state observed in these compounds. On the other hand, it is plausible that the oxides should have a larger J_2 thanks to the shorter Yb-Yb distances. Whereas the field-induced order in $NaYbO_2$ may be still of the *uud* type, the lower value of J_1 in $KYbO_2$ should facilitate the $J_2/J_1 > 0.125$ regime and the $\frac{1}{2}$ plateau typical of the *uuud* order. Moreover, if the coupling J_2 is sensitive to the linearity of the Yb-O…O-Yb pathway, as expected from the Cu^{2+} compounds [47], one should anticipate the increased J_2 in $KYbO_2$ with the Yb-O-O angle of 138.6° compared to $NaYbO_2$ with its angle of 137.8°. This will further increase the J_2/J_1 ratio.

The assignment of $J_2/J_1 > 0.125$ calls for a further theoretical study of this regime. The experimental magnetization curve may serve as a useful reference, as it shows a characteristic nonlinear behavior between zero field and the onset of the plateau [Fig. 3(b)], as opposed to the classical linear behavior. Another interesting aspect is the possible onset of magnetic order already at zero field that may be inferred from the divergence of the ESR linewidth (Fig. 2). The scale of this tentative transition is given by $T_c = 0.15$ K that, however, lies well below the temperature range covered in the present work.

In summary, the A-site substitution in the QSL candidate $NaYbO_2$ leads to an anisotropic tensile strain and affects different aspects of the magnetism. Magnetic couplings are reduced following the increase in the Yb-O-Yb angles. This results in the lower saturation field and in the shift of the intermediate field-induced ordered state toward lower fields and temperatures. Additionally, the change in the local environment of Yb^{3+} renders the *g* tensor almost isotropic. A partial A-site substitution may then be a viable strategy for a fine tuning of magnetic interactions in triangular antiferromagnets. We have also shown that $KYbO_2$ develops the $\frac{1}{2}$ magnetization plateau, which is indicative of the *uuud* field-induced order and may signal the sizable second-neighbor coupling J_2 in this compound.

ACKNOWLEDGMENTS

We thank Aleksandr Missiul, Francois Fauth, and Alexander Zubtsovskii for their help with the data collection at

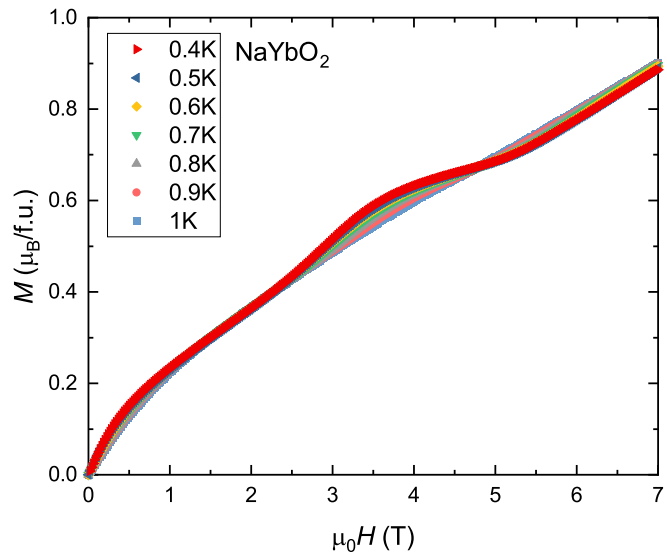

FIG. 7. Low-temperature magnetization of $NaYbO_2$. The plateau is located between 3 and 5.5 T at about half of the saturation magnetization.

MSPD. This work was funded by the German Research Foundation (DFG) via Project No. 107745057 (TRR80). We also acknowledge the support of the HLD at HZDR, member of European Magnetic Field Laboratory (EMFL).

APPENDIX: ADDITIONAL DATA FOR $NaYbO_2$

For a systematic comparison with $KYbO_2$, we performed additional measurements on $NaYbO_2$. These measurements extend the data that have been reported by us earlier [17]. Fig. 5 shows specific heat of $NaYbO_2$ and confirms the absence of magnetic order in zero field. Applying magnetic field induces long-range order manifested by a λ-type anomaly above 3 T. Similar to $KYbO_2$, the anomaly shifts to higher temperatures when increasing the field up to 5 T, while for higher fields this trend is reversed. The position of this peak is used to track the phase boundary shown in Fig. 6. Additionally, the second peak appears above 6 T as a shoulder on the lower-temperature side, similar to the data reported in Ref. [37]. We interpret this second peak as the transition induced by the field $H \| c$ because the lower component of the g-tensor weakens the effect of the out-of-plane field and, correspondingly, a higher field strength would be needed to stabilize field-induced order. Since $g_\perp = 3.28(8)$ of $NaYbO_2$ is similar to the isotropic $g = 3.08(3)$ of $KYbO_2$, while $g_\parallel = 1.75(3)$ is much lower, we used the first peak when tracing the phase boundary. We also measured the low-temperature $M(H)$ curves for $NaYbO_2$ (Fig. 7) and traced the field range of the plateau using maxima and minima in the second derivative.

[1] P. Anderson, Resonating valence bonds: A new kind of insulator? Mater. Res. Bull. **8**, 153 (1973).

[2] X.-G. Wen, Choreographed entanglement dances: Topological states of quantum matter, Science **363**, eaal3099 (2019).

[3] C. Broholm, R. J. Cava, S. A. Kivelson, D. G. Nocera, M. R. Norman, and T. Senthil, Quantum spin liquids, Science **367**, eaay0668 (2020).

[4] J. R. Chamorro, T. M. McQueen, and T. T. Tran, Chemistry of quantum spin liquids, Chem. Rev. **121**, 2898 (2021).

[5] Y. Li, G. Chen, W. Tong, L. Pi, J. Liu, Z. Yang, X. Wang, and Q. Zhang, Rare-Earth Triangular Lattice Spin Liquid: A Single-Crystal Study of $YbMgGaO_4$, Phys. Rev. Lett. **115**, 167203 (2015).

[6] Y. Li, D. Adroja, P. K. Biswas, P. J. Baker, Q. Zhang, J. Liu, A. A. Tsirlin, P. Gegenwart, and Q. Zhang, Muon spin relaxation evidence for the U(1) quantum spin-liquid ground state in the triangular antiferromagnet $YbMgGaO_4$, Phys. Rev. Lett. **117**, 097201 (2016).

[7] Z. Ding, Z. Zhu, J. Zhang, C. Tan, Y. Yang, D. E. MacLaughlin, and L. Shu, Persistent spin dynamics and absence of spin freezing in the $H-T$ phase diagram of the two-dimensional triangular antiferromagnet $YbMgGaO_4$, Phys. Rev. B **102**, 014428 (2020).

[8] Y. Li, H. Liao, Z. Zhang, S. Li, F. Jin, L. Ling, L. Zhang, Y. Zou, L. Pi, Z. Yang, J. Wang, Z. Wu, and Q. Zhang, Gapless quantum spin liquid ground state in the two-dimensional spin-1/2 triangular antiferromagnet $YbMgGaO_4$, Sci. Rep. **5**, 16419 (2015).

[9] J. A. M. Paddison, M. Daum, Z. Dun, G. Ehlers, Y. Liu, M. B. Stone, H. Zhou, and M. Mourigal, Continuous excitations of the triangular-lattice quantum spin liquid $YbMgGaO_4$, Nat. Phys. **13**, 117 (2017).

[10] Y. Shen, Y.-D. Li, S. Shen, B. Pan, Q. Wang, H. C. Walker, P. Steffens, M. Boehm, Y. Hao, D. L. Quintero-Castro, L. W. Harriger, M. D. Frontzek, L. Hao, S. Meng, Q. Zhang, G. Chen, and J. Zhao, Evidence for a spinon Fermi surface in a triangular-lattice quantum-spin-liquid candidate, Nature (London) **540**, 559 (2016).

[11] Y. Li, D. Adroja, D. Voneshen, R. I. Bewley, Q. Zhang, A. A. Tsirlin, and P. Gegenwart, Nearest-neighbour resonating valence bonds in $YbMgGaO_4$, Nat. Commun. **8**, 15814 (2017).

[12] Y. Li, S. Bachus, B. Liu, I. Radelytskyi, A. Bertin, A. Schneidewind, Y. Tokiwa, A. A. Tsirlin, and P. Gegenwart, Rearrangement of Uncorrelated Valence Bonds Evidenced by Low-Energy Spin Excitations in $YbMgGaO_4$, Phys. Rev. Lett. **122**, 137201 (2019).

[13] Y. Li, D. Adroja, R. I. Bewley, D. Voneshen, A. A. Tsirlin, P. Gegenwart, and Q. Zhang, Crystalline Electric-Field Randomness in the Triangular Lattice Spin-Liquid $YbMgGaO_4$, Phys. Rev. Lett. **118**, 107202 (2017).

[14] Z. Zhu, P. A. Maksimov, S. R. White, and A. L. Chernyshev, Disorder-Induced Mimicry of a Spin Liquid in $YbMgGaO_4$, Phys. Rev. Lett. **119**, 157201 (2017).

[15] Y. Li, P. Gegenwart, and A. A. Tsirlin, Spin liquids in geometrically perfect triangular antiferromagnets, J. Phys.: Condens. Matter **32**, 224004 (2020).

[16] M. Baenitz, P. Schlender, J. Sichelschmidt, Y. A. Onykiienko, Z. Zangeneh, K. M. Ranjith, R. Sarkar, L. Hozoi, H. C. Walker, J.-C. Orain, H. Yasuoka, J. van den Brink, H. H. Klauss, D. S. Inosov, and T. Doert, $NaYbS_2$: A planar spin-$\frac{1}{2}$ triangular-lattice magnet and putative spin liquid, Phys. Rev. B **98**, 220409(R) (2018).

[17] L. Ding, P. Manuel, S. Bachus, F. Grußler, P. Gegenwart, J. Singleton, R. D. Johnson, H. C. Walker, D. T. Adroja, A. D. Hillier, and A. A. Tsirlin, Gapless spin-liquid state in the structurally disorder-free triangular antiferromagnet $NaYbO_2$, Phys. Rev. B **100**, 144432 (2019).

[18] K. M. Ranjith, S. Luther, T. Reimann, B. Schmidt, P. Schlender, J. Sichelschmidt, H. Yasuoka, A. M. Strydom, Y. Skourski, J. Wosnitza, H. Kühne, T. Doert, and M. Baenitz, Anisotropic field-induced ordering in the triangular-lattice quantum spin liquid $NaYbSe_2$, Phys. Rev. B **100**, 224417 (2019).

[19] M. M. Bordelon, E. Kenney, C. Liu, T. Hogan, L. Posthuma, M. Kavand, Y. Lyu, M. Sherwin, N. P. Butch, C. Brown, M. J. Graf, L. Balents, and S. D. Wilson, Field-tunable quantum disordered ground state in the triangular-lattice antiferromagnet $NaYbO_2$, Nat. Phys. **15**, 1058 (2019).

[20] R. Sarkar, P. Schlender, V. Grinenko, E. Haeussler, P. J. Baker, T. Doert, and H.-H. Klauss, Quantum spin liquid ground state in the disorder free triangular lattice $NaYbS_2$, Phys. Rev. B **100**, 241116(R) (2019).

[21] B. Schmidt, J. Sichelschmidt, K. M. Ranjith, T. Doert, and M. Baenitz, Yb delafossites: Unique exchange frustration of $4f$ spin-$\frac{1}{2}$ moments on a perfect triangular lattice, Phys. Rev. B **103**, 214445 (2021).

[22] Z. Zhang, X. Ma, J. Li, G. Wang, D. T. Adroja, T. P. Perring, W. Liu, F. Jin, J. Ji, Y. Wang, Y. Kamiya, X. Wang, J. Ma, and Q. Zhang, Crystalline electric field excitations in the quantum spin liquid candidate $NaYbSe_2$, Phys. Rev. B **103**, 035144 (2021).

[23] P.-L. Dai, G. Zhang, Y. Xie, C. Duan, Y. Gao, Z. Zhu, E. Feng, Z. Tao, C.-L. Huang, H. Cao, A. Podlesnyak, G. E. Granroth, M. S. Everett, J. C. Neuefeind, D. Voneshen, S. Wang, G. Tan, E. Morosan, X. Wang, H.-Q. Lin *et al.*, Spinon Fermi Surface Spin Liquid in a Triangular Lattice Antiferromagnet $NaYbSe_2$, Phys. Rev. X **11**, 021044 (2021).

[24] Z. Zhang, J. Li, W. Liu, Z. Zhang, J. Ji, F. Jin, R. Chen, J. Wang, X. Wang, J. Ma, and Q. Zhang, Effective magnetic Hamiltonian at finite temperatures for rare-earth chalcogenides, Phys. Rev. B **103**, 184419 (2021).

[25] Z. H. Zhu, B. L. Pan, L. P. Nie, J. M. Ni, Y. X. Yang, C. S. Chen, Y. Y. Huang, E. J. Cheng, Y. J. Yu, A. D. Hillier, X. H. Chen, T. Wu, Y. Zhou, S. Y. Li, and L. Shu, Fluctuating magnetic droplets immersed in a sea of quantum spin liquid, arXiv:2112.06523.

[26] J. Xing, L. D. Sanjeewa, J. Kim, G. R. Stewart, A. Podlesnyak, and A. S. Sefat, Field-induced magnetic transition and spin fluctuations in the quantum spin-liquid candidate $CsYbSe_2$, Phys. Rev. B **100**, 220407(R) (2019).

[27] J. Xing, L. D. Sanjeewa, J. Kim, G. R. Stewart, M.-H. Du, F. A. Reboredo, R. Custelcean, and A. S. Sefat, Crystal synthesis and frustrated magnetism in triangular lattice $CsRESe_2$ (RE = La-Lu): Quantum spin liquid candidates $CsCeSe_2$ and $CsYbSe_2$, ACS Mater. Lett. **2**, 71 (2020).

[28] J. Xing, L. D. Sanjeewa, A. F. May, and A. S. Sefat, Synthesis and anisotropic magnetism in quantum spin liquid candidates $AYbSe_2$ (A = K and Rb), APL Mater. **9**, 111104 (2021).

[29] A. O. Scheie, E. A. Ghioldi, J. Xing, J. A. M. Paddison, N. E. Sherman, M. Dupont, D. Abernathy, D. M. Pajerowski, S.-S. Zhang, L. O. Manuel, A. E. Trumper, C. D. Pemmaraju, A. S. Sefat, D. S. Parker, T. P. Devereaux, J. E. Moore, C. D. Batista, and D. A. Tennant, Witnessing quantum criticality and entanglement in the triangular antiferromagnet $KYbSe_2$, arXiv:2109.11527.

[30] E. Häußler, J. Sichelschmidt, M. Baenitz, E. C. Andrade, M. Vojta, and T. Doert, Diluting a triangular-lattice spin liquid: Synthesis and characterization of $NaYb_{1-x}Lu_xS_2$ single crystals, Phys. Rev. Mater. **6**, 046201 (2022).

[31] B. Dong, Y. Doi, and Y. Hinatsu, Structure and magnetic properties of ternary potassium lanthanide oxides $KLnO_2$ (Ln=Y, Nd, Sm-Lu), J. Alloys Compd. **453**, 282 (2008).

[32] M. M. Bordelon, C. Liu, L. Posthuma, E. Kenney, M. J. Graf, N. P. Butch, A. Banerjee, S. Calder, L. Balents, and S. D. Wilson, Frustrated Heisenberg $J_1 - J_2$ model within the stretched diamond lattice of $LiYbO_2$, Phys. Rev. B **103**, 014420 (2021).

[33] F. Fauth, I. Peral, C. Popescu, and M. Knapp, The new Material Science Powder Diffraction beamline at ALBA synchrotron, Powder Diffr. **28**, S360 (2013).

[34] M. Majumder, G. Simutis, I. E. Collings, J.-C. Orain, T. Dey, Y. Li, P. Gegenwart, and A. A. Tsirlin, Persistent spin dynamics in the pressurized spin-liquid candidate $YbMgGaO_4$, Phys. Rev. Res. **2**, 023191 (2020).

[35] J. Sichelschmidt, B. Schmidt, P. Schlender, S. Khim, T. Doert, and M. Baenitz, Effective spin-1/2 moments on a Yb^{3+} triangular lattice: An ESR study, JPS Conf. Proc. **30**, 011096 (2020).

[36] J. Sichelschmidt, P. Schlender, B. Schmidt, M. Baenitz, and T. Doert, Electron spin resonance on the spin-1/2 triangular magnet $NaYbS_2$, J. Phys.: Condens. Matter **31**, 205601 (2019).

[37] K. M. Ranjith, D. Dmytriieva, S. Khim, J. Sichelschmidt, S. Luther, D. Ehlers, H. Yasuoka, J. Wosnitza, A. A. Tsirlin, H. Kühne, and M. Baenitz, Field-induced instability of the quantum spin liquid ground state in the $J_{\text{eff}} = \frac{1}{2}$ triangular-lattice compound $NaYbO_2$, Phys. Rev. B **99**, 180401(R) (2019).

[38] M. Heinrich, H. A. Krug von Nidda, A. Loidl, N. Rogado, and R. J. Cava, Potential Signature of a Kosterlitz-Thouless Transition in $BaNi_2V_2O_8$, Phys. Rev. Lett. **91**, 137601 (2003).

[39] M. Hemmida, H. A. Krug von Nidda, N. Büttgen, A. Loidl, L. K. Alexander, R. Nath, A. V. Mahajan, R. F. Berger, R. J. Cava, Y. Singh, and D. C. Johnston, Vortex dynamics and frustration in two-dimensional triangular chromium lattices, Phys. Rev. B **80**, 054406 (2009).

[40] K. Somesh, Y. Furukawa, G. Simutis, F. Bert, M. Prinz-Zwick, N. Büttgen, A. Zorko, A. A. Tsirlin, P. Mendels, and R. Nath, Universal fluctuating regime in triangular chromate antiferromagnets, Phys. Rev. B **104**, 104422 (2021).

[41] A. O. Scheie, Y. Kamiya, H. Zhang, S. Lee, A. J. Woods, M. G. Gonzalez, B. Bernu, J. Xing, Q. Huang, Q. M. Zhang, J. Ma, E. S. Choi, D. M. Pajerowski, H. Zhou, A. S. Sefat, L. Messio, R. Movshovich, C. D. Batista, and D. A. Tennant, Non-linear magnons and exchange hamiltonians of delafossite proximate quantum spin liquids, arXiv:2207.14785.

[42] T. Xie, A. A. Eberharter, J. Xing, S. Nishimoto, M. Brando, P. Khanenko, J. Sichelschmidt, A. A. Turrini, D. G. Mazzone, P. G. Naumov, L. D. Sanjeewa, N. Harrison, A. S. Sefat, B. Normand, A. M. Läuchli, A. Podlesnyak, and S. E. Nikitin, Complete field-induced spectral response of the spin-1/2 triangular-lattice antiferromagnet $CsYbSe_2$, arXiv:2210.04928.

[43] R. M. Moon, H. R. Child, W. C. Koehler, and L. J. Raubenheimer, Magnetic structure of Er_2O_3 and Yb_2O_3, J. Appl. Phys. **38**, 1383 (1967).

[44] X. Z. Liu, O. Prokhnenko, D. Yamamoto, M. Bartkowiak, N. Kurita, and H. Tanaka, Microscopic evidence of a quantum magnetization process in the $S = \frac{1}{2}$ triangular-lattice Heisenberg-like antiferromagnet $Ba_3CoSb_2O_9$, Phys. Rev. B **100**, 094436 (2019).

[45] M. Ye and A. V. Chubukov, Half-magnetization plateau in a Heisenberg antiferromagnet on a triangular lattice, Phys. Rev. B **96**, 140406(R) (2017).

[46] M. Ye and A. V. Chubukov, Quantum phase transitions in the Heisenberg $J_1 - J_2$ triangular antiferromagnet in a magnetic field, Phys. Rev. B **95**, 014425 (2017).

[47] D. A. Prishchenko, A. A. Tsirlin, V. Tsurkan, A. Loidl, A. Jesche, and V. G. Mazurenko, Antiferroelectric instability in the kagome francisites $Cu_3Bi(SeO_3)_2O_2X$ (X = Cl, Br), Phys. Rev. B **95**, 064102 (2017).